Fission of light actinides: ^{232}Th(n, f) and ^{231}Pa(n, f) reactions

M. Sin[*]

Nuclear Physics Department, University of Bucharest, P.O. Box MG-11, Bucharest-Magurele, Romania

R. Capote

NAPC-Nuclear Data Section, International Atomic Energy Agency, Vienna, Austria

A. Ventura

Ente Nuove Tecnologie, Energia e Ambiente and Istituto Nazionale di Fisica Nucleare, Bologna, Italy

M. Herman and P. Obložinský

National Nuclear Data Center, Brookhaven National Laboratory, Upton, New York 11973, USA

A model to describe fission on light actinides, which takes into account transmission through a triple-humped fission barrier with absorption, is proposed. The fission probability derived in the WKB approximation within an optical model for fission has been incorporated into the statistical model of nuclear reactions. The complex resonant structure in the first-chance neutron-induced fission cross sections of ^{232}Th and ^{231}Pa nuclei has been reproduced by the proposed model. Consistent sets of parameters describing the triple-humped fission barriers of ^{233}Th and ^{232}Pa have been obtained. The results confirm the attribution of the gross resonant structure in the fission probability of these light actinides to partially damped vibrational states in the second well and undamped vibrational states in the third well of the corresponding fission barriers.

I. INTRODUCTION

Scientific interest in the fission of light actinides is mainly due to the effect known as the "thorium anomaly" [1]. It has been demonstrated that in the thorium region, second-order shell effects split the outer fission barrier giving the so-called triple-humped structure. Triple-humped barriers, allowing the existence of exotic hyperdeformed class III vibrational states, could explain the significant structure in the fission cross section of Th, Pa, and light U isotopes. Many theoretical and experimental studies have been dedicated to this subject in the last decades (e.g., Ref. [2–5]). Recently, a triple-humped barrier was proposed to be used to describe neutron-induced fission on ^{238}U [6]. Different types of analysis resulted in different predictions of the fission barrier parameters, but none of these papers present calculations of the fission cross section reproducing the resonant structure of the measured data in an extended energy range. Additional motivation for our work is the importance of light actinides for the accelerator-driven system (ADS) and innovative fuel cycle concepts based on thorium fuel [7]. Knowledge of accurate neutron-induced fission cross sections is crucially important for the design of various reactor systems. During recent years, several studies of neutron-induced reactions on thorium and protactinium are being discussed in the framework of the on-going IAEA Coordinated Research Program [7], including those published by Maslov [8] and Han and Zhang [9], who used the triple-humped fission barrier. However, uncoupled fission barriers were employed, meaning that the resonant structure present in the experimental data could only be reproduced on average.

The aim of this paper is to propose a fission formalism based on the optical model for fission [3,10] extended to include triple-humped barriers. A consistent way to integrate this formalism, needed for light actinides, within the statistical model of nuclear reactions will be presented. Its capabilities to provide information on the fission barrier parameters and to accurately predict fission cross sections will be tested on the first-chance neutron-induced fission on even-even ^{232}Th and odd-even ^{231}Pa targets.

Section II of this paper provides a general description of the fission model for light actinides and its integration within the statistical model of nuclear reactions. Expressions used for fission barrier parametrization, fission coefficients corresponding to different transmission mechanisms, and decay probabilities for fission and competing processes are given. Section III describes the application of the model to neutron-induced fission on thorium and protactinium up to about 5 MeV neutron incident energy. Finally, Sec. IV presents our conclusions.

II. FISSION MODEL FOR LIGHT ACTINIDES

The optical model for fission was developed to describe the resonant structure of the fission cross section at subbarrier excitation energies. The structure appears because of resonant transmission through vibrational states in the second well of a double-humped fission barrier. In this model, the damping of the class II vibrational states and their coupling to class I states (i.e., the absorption of the incident flux in the isomeric
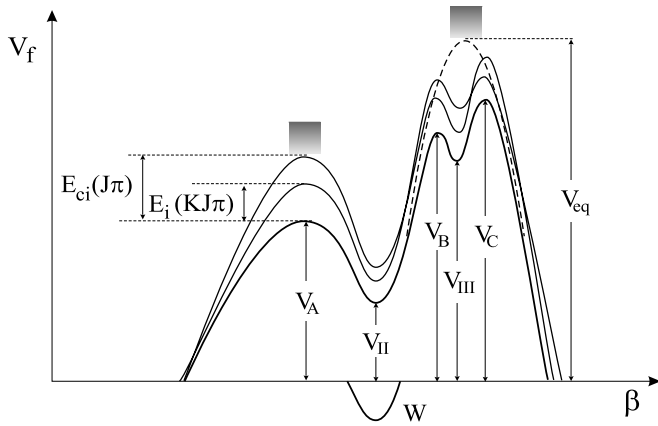
_____
[*]Electronic address: msin@pcnet.ro

FIG. 1. Triple-humped fission barrier parametrization.

well) are considered by introducing an imaginary potential in the deformation range corresponding to the second minimum. Generalized relations for the decay probabilities accounting for all the possible transmission mechanisms through the fission barriers were deduced in Refs. [10–12]. The fission coefficients entering these relations are determined within the WKB approximation [13].

The optical model for fission, so far applied to the nuclei exhibiting a double-humped fission barrier [10,11], is extended here to light actinides featuring a complex triple-humped fission barrier. The optical model for fission considers the possible transmission mechanisms using a complex potential $(V_f = V + iW)$ to describe the unidimensional multihumped fission barrier (Fig. 1). The real part of the barriers associated with the discrete transition states are parametrized by smoothly joined parabolas as a function of the deformation β along the fission path

$$V_i(\beta) = E_{fi} + (-1)^i \frac{1}{2}\mu\hbar^2\omega_i^2(\beta - \beta_i)^2, \qquad (1)$$

where i runs from 1 to 5 for a three-humped barrier. The energies E_{fi} represent maxima of V_i in odd regions (humps) and minima in even regions (wells), β_i are the corresponding abscissae, the harmonic oscillator frequencies ω_i define the curvature of each parabola, and μ is the inertial mass parameter, assumed independent of β and approximated by the semiempirical expression $\mu \approx 0.054A^{5/3}$ MeV^{-1} [14], where A is the mass number.

The discrete transition states are rotational levels built on vibrational or noncollective bandheads, characterized by a given set of quantum numbers (angular momentum J, parity π, and angular momentum projection on the nuclear symmetry axis K) with the excitation energies

$$E_i(KJ\pi) = E_{fi} + \epsilon_i(K\pi) + \frac{\hbar^2}{2I_i}[J(J+1) - K(K+1) \\ + s(-1)^{J+1/2}(J+1/2)\delta_{K,1/2}], \qquad (2)$$

where $\epsilon_i(K\pi)$ are the bandhead energies, $\hbar^2/2I$ are the rotational constants, and s is the decoupling parameter for $K = 1/2$ bands. A parabolic barrier with height $E_i(KJ\pi)$ and curvature $\hbar\omega_i$ is associated with each transition state. Relation (2) is obtained in the strong coupling limit of the particle-rotor

model for odd-mass nuclei and is valid for even-even nuclei as well, since, in the latter case, K is integer and the Kronecker delta in the r.h.s. is obviously zero. In the present work, it will be applied to odd-odd nuclei, too, by neglecting any residual proton-neutron interaction.

The transition state spectrum has a discrete component up to a certain energy E_{ci}, above which it is continuous and described by the level density functions $\rho_i(EJ\pi)$, accounting for collective enhancements specific to the nuclear shape symmetry at each saddle point. For the case of a triple-humped barrier, it is reasonable to assume that with increasing excitation energy, the shell effects, which cause splitting of the outer hump, decrease and the outer humps lump into a single one. Therefore, in the present formalism, triple-humped barriers are associated only with discrete transition states. Accordingly, the continuum contribution to the fission coefficient is calculated considering a double-humped barrier with the second peak representing a single barrier equivalent to the two outer humps (Fig. 1). The parameters of the equivalent barrier are determined imposing equal transmission.

The negative imaginary potential iW is introduced in the deformation range corresponding to the second well to simulate damping of the class II vibrational states causing absorption of the incoming flux in this well. In the present formalism, the third well is supposed to be shallow enough to neglect damping of class III vibrational states. The strength W is assumed to be an energy-dependent function of the deformation β

$$W(\beta) = -\alpha(E)[E - V(\beta)]. \qquad (3)$$

The $\alpha(E)$ parameter, which controls the strength of the imaginary part of the fission potential, should be chosen to fit the width of the resonances in the subbarrier fission cross section and to be consistent with physical values for the transmission coefficients at higher energies.

In the following sections, the humps will be denoted with capital letters A, B, C ($i = 1, 3, 5$) and the wells with Roman numerals II ($i = 2$) and III ($i = 4$).

A. Fission coefficients for triple-humped barrier

Figure 2 shows the transmission mechanisms through a triple-humped fission barrier for two excitation energies, one lower and one higher than the top of the first hump. The incoming flux can be transmitted directly through the barrier or absorbed in the isomeric well. The fraction absorbed in the isomeric well can (i) be reemitted in the fission channel by direct transmission through the second and third hump, (ii) return back to a class I state, or (iii) undergo γ transition to the isomeric state; the isomeric state, in turn, can decay by delayed (isomeric) fission or by shape transition to class I states.

Accordingly, the fission coefficient through one discrete triple-humped barrier is the sum of two terms: the first, $T_{dir}(EKJ\pi)$, representing direct transmission, and the second,
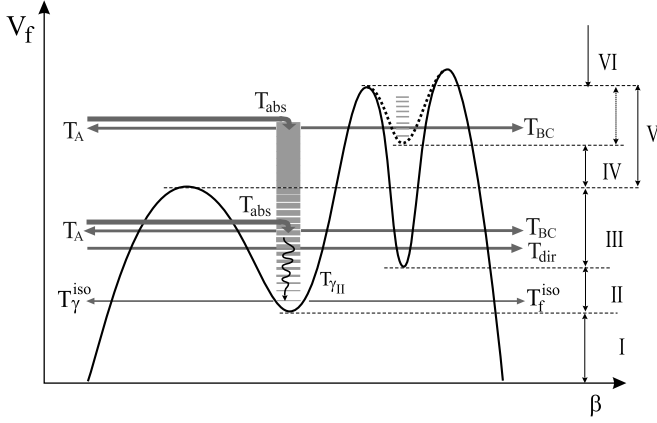
FIG. 2. Mechanisms of transmission across the triple-humped fission barrier.

$T_{\text{ind}}(EKJ\pi)$, representing the indirect transmission given by the product of the absorption coefficient $T_{\text{abs}}(EKJ\pi)$, and the branching ratio for indirect prompt and delayed (isomeric) fission [10,15]

$$
\begin{aligned}
T_f(EKJ\pi) &= T_{\text{dir}}(EKJ\pi) + T_{\text{ind}}(EKJ\pi) \\
&= T_{\text{dir}}(EKJ\pi) + T_{\text{abs}}(EKJ\pi) \\
&\quad \times \frac{T_{BC}(EKJ\pi) + RT_{\gamma II}(EJ\pi)}{T_A(EKJ\pi) + T_{BC}(EKJ\pi) + T_{\gamma II}(EJ\pi)},
\end{aligned}
\tag{4}
$$

where E is the excitation energy, $T_A(EKJ\pi)$ is the transmission coefficient through the first peak, $T_{BC}(EKJ\pi)$ is the direct transmission coefficient through the outer peaks, $T_{\gamma II}(EJ\pi)$ describes γ decay in the isomeric well, and R is the branching ratio for fission of the isomeric state. In the case of the light actinides, R is very small and can be neglected. Considering that γ decay could make a sizable contribution only at very low excitation energies in the isomeric well, $T_{\gamma II}(EJ\pi)$ will be neglected as well.

1. WKB relations for fission coefficients

The transmission coefficients entering Eq. (4) are expressed in first-order WKB approximation in terms of the momentum integrals for the humps [13,16], that is,

$$
K_j = \pm \left| \int_{a_j}^{b_j} [2\mu(E - V_j(\beta))/\hbar^2]^{1/2} d\beta \right|, \quad j = A, B, C,
\tag{5}
$$

where the $+$ sign is taken when the excitation energy is lower than the hump under consideration and the $-$ when it is higher. In the latter case, the intercepts are complex conjugate ($b_j = a_j^*$), and the WKB approximation is valid when their imaginary parts are small, i.e., for energies slightly higher than the hump. The single-hump transmission coefficients T_j turn out to be

$$
T_j = \frac{1}{1 + \exp(2K_j)}, \quad j = A, B, C.
\tag{6}
$$

As is known, in the case of a single parabolic barrier, $V(\beta) = V_0 - 1/2\mu\omega^2\beta^2$, formula (6) yields the well-known Hill-Wheeler transmission coefficient [1]

$$
T_{\text{HW}} = \frac{1}{1 + \exp\left(2\pi \frac{V_0 - E}{\hbar\omega}\right)},
\tag{7}
$$

which is an exact result.

In the intermediate wells, when the intercepts a_j and b_j are real, the momentum integrals depending on the real parts of the potential are approximated as

$$
\nu_j = \int_{a_i}^{b_i} [2\mu(E - V_i(\beta))/\hbar^2]^{1/2} d\beta,
\tag{8}
$$

where $j = 1$ for $i = \text{II}$, and $j = 2$ for $i = \text{III}$; while for the imaginary potential in the isomeric well, one obtains [15]

$$
\delta = -\left(\frac{\mu}{2\hbar^2}\right)^{1/2} \int_{a_{\text{II}}}^{b_{\text{II}}} \frac{W(\beta)}{(E - V_{\text{II}}(\beta))^{1/2}} d\beta.
\tag{9}
$$

The general expression for the direct transmission coefficient of a triple-humped barrier with an imaginary component in the isomeric well is a simple generalization of that obtained for a real three-humped barrier in Ref. [17]

$$
T_{\text{dir}} = \frac{T_A T_B T_C}{A_T + B_T \cos(2(\nu_1 - \nu_2)) + C_T \cos(2(\nu_1 + \nu_2)) + D_T \cos(2\nu_1) + E_T \cos(2\nu_2)},
\tag{10}
$$

where

$$
\begin{aligned}
A_T &= e^{-2\delta}(1 - T_A)(1 - T_B) + e^{2\delta}(1 - T_B)(1 - T_C) \\
&\quad + e^{-2\delta}(1 - T_A)(1 - T_C) + e^{2\delta}, \\
B_T &= 2(1 - T_A)^{1/2}(1 - T_B)(1 - T_C)^{1/2}, \\
C_T &= 2(1 - T_A)^{1/2}(1 - T_C)^{1/2}, \\
D_T &= 2(1 - T_A)^{1/2}(1 - T_B)^{1/2}(2 - T_C), \\
E_T &= 2(1 - T_B)^{1/2}(1 - T_C)^{1/2}[e^{-2\delta}(1 - T_A) + e^{2\delta}],
\end{aligned}
\tag{11}
$$

which reduces to the form of Ref. [17] in the $\delta \to 0$ limit.

The reflection coefficient T_{refl}, is conveniently expressed in terms of the transmission T_{dir} as

$$
\begin{aligned}
T_{\text{refl}} &= \frac{T_{\text{dir}}}{T_A T_B T_C}[A_R + B_R \cos(2(\nu_1 - \nu_2)) \\
&\quad + C_R \cos(2(\nu_1 + \nu_2)) + D_R \cos(2\nu_1) + E_R \cos(2\nu_2)],
\end{aligned}
\tag{12}
$$

where

$$
\begin{aligned}
A_R &= e^{-2\delta}(2 - T_B - T_C) \\
&\quad + e^{2\delta}(1 - T_A)[(1 - T_B)(1 - T_C) + 1], \\
B_R &= 2(1 - T_A)^{1/2}(1 - T_B)(1 - T_C)^{1/2} = B_T, \\
C_R &= 2(1 - T_A)^{1/2}(1 - T_C)^{1/2} = C_T, \\
D_R &= 2(1 - T_A)^{1/2}(1 - T_B)^{1/2}(2 - T_C) = D_T, \\
E_R &= 2(1 - T_B)^{1/2}(1 - T_C)^{1/2}[e^{-2\delta} + e^{2\delta}(1 - T_A)].
\end{aligned}
\tag{13}
$$

Since the fission barrier is complex, there is a nonzero absorption coefficient

$$
\begin{aligned}
T_{\text{abs}} &= 1 - T_{\text{dir}} - T_{\text{refl}} \\
&= \frac{T_{\text{dir}}}{T_B T_C}[(2 - T_B - T_C + T_B T_C)e^{2\delta} \\
&\quad + (-2 + T_B + T_C)e^{-2\delta} - T_B T_C \\
&\quad + 2(1 - T_B)^{1/2}(1 - T_C)^{1/2}(e^{2\delta} - e^{-2\delta})].
\end{aligned}
\tag{14}
$$

These general relations for the transmission coefficients through a triple-humped barrier with an imaginary component in the isomeric well take particular forms in the excitation energy regions indicated in Fig. 2, as detailed in Appendix A.

2. Addendum on parabolic cylinder functions

It is worthwhile to make a short comment on the use of the WKB approximation in the transmission and reflection by a multiple-humped parabolic barrier, which is exactly solvable, with wave functions expressible in terms of parabolic cylinder functions [18,19]. The exact form of the transmission coefficient of a real three-humped fission barrier is given in Ref. [20], and its generalization to a complex barrier is straightforward. In the case of a real barrier, however, it was already proved that the WKB formulas yield a good approximation to exact results in the nontrivial energy range below and at the tops of the barrier peaks [21]. Therefore, the WKB approximation has been adopted in the present work in order not to burden a complicated set of nuclear reaction codes like EMPIRE with routines for parabolic cylinder functions of complex argument, and also to keep a more physical insight on partial or total damping of vibrational resonances, essentially governed by the δ parameter of the WKB formulas given above; the damping effects would be less transparent in a fully numerical evaluation of transmission and absorption coefficients.

3. Total fission coefficients

The total fission coefficient for a certain spin and parity which enters the statistical model of nuclear reactions is the sum of the contributions of all bands containing levels with the same spin and parity. In the description of fission cross sections, one can consider two extreme limits: the first limit assumes that fission mainly proceeds through discrete transition states characterized by well-defined values of K and is known as the "no K mixing" approximation; the second limit considers that the excitation of internal degrees of freedom in

the second well makes it possible for the nucleus to change its K value during the time the energy is bound in internal motions, and this effect is referred to as "full K mixing." The effect of these approximations on the fission probability is very small, but they can affect significantly the angular correlations of the fission fragments [10]. The appropriate choice for the purpose of nuclear data evaluation, i.e., computation of the fission cross section in a broad energy range, is the "full K mixing" approximation, not only for physical reasons, but also because it can be applied to any excitation energy. On the other hand, if the fission cross section is studied simultaneously with the angular distributions of fission fragments in the narrow energy window where class III vibrational states can be excited, the no K-mixing assumption can be made, in order to extract information on the $K\pi$ quantum number of the class III states under investigation.

Formally, full K mixing is described by adding the absorption from different transition states irrespective of the associated K value into a quantity preserving the spin J and parity π. The main consequence is that the second term in Eq. (4), describing the prompt indirect fission (i.e., the reemission into the fission channel after absorption in the isomeric well), becomes

$$
\begin{aligned}
T_{\text{ind}}(EKJ\pi) &= \sum_{K'' \leqslant J} T_{\text{abs}}(EK''J\pi) \\
&\quad \times \frac{T_{BC}(EKJ\pi)}{\sum_{K'' \leqslant J}[T_A(EK''J\pi) + T_{BC}(EK''J\pi)]}.
\end{aligned}
\tag{15}
$$

In this approximation, the total fission coefficient for a certain discrete state characterized by quantum numbers $J\pi$ reads

$$
\begin{aligned}
T_f(EJ\pi) &= \sum_{K \leqslant J} T_f(EKJ\pi) \\
&= \sum_{K \leqslant J}[T_{\text{dir}}(EKJ\pi) + T_{\text{ind}}(EKJ\pi)] \\
&= T_{\text{dir}}(EJ\pi) + T_{\text{abs}}(EJ\pi) \\
&\quad \times \frac{T_{BC}(EJ\pi)}{T_A(EJ\pi) + T_{BC}(EJ\pi)}.
\end{aligned}
\tag{16}
$$

The total transmission coefficient through one hump is the sum of two contributions corresponding to the discrete and continuous part of the transition state spectrum, that is,

$$
\begin{aligned}
T_A(EJ\pi) &= \sum_{K \leqslant J} T_A(EKJ\pi) \\
&\quad + \int_{E_{cA}}^{\infty} \frac{\rho_A(\varepsilon J\pi)d\varepsilon}{1 + \exp\left[-\frac{2\pi}{\hbar\omega_A}(E - V_A - \varepsilon)\right]}.
\end{aligned}
\tag{17}
$$

The total direct transmission through the outer humps is the sum of the transmissions through discrete barriers and the

continuum built above the equivalent barrier such that

$$T_{BC}(EJ\pi) = \sum_{K \leqslant J} T_{BC}(EKJ\pi)$$
$$+ \int_{E_{ceq}}^{\infty} \frac{\rho_{eq}(\varepsilon J\pi)d\varepsilon}{1 + \exp\left[-\frac{2\pi}{\hbar\omega_{eq}}(E - V_{eq} - \varepsilon)\right]}. \quad (18)$$

By increasing the excitation energy, the strength of the imaginary potential increases, and the entire flux transmitted through the inner hump is absorbed in the second (isomeric) well ($T_{abs} \to T_A$), and the direct transmission through the entire barrier disappears ($T_{dir} \to 0$). Therefore, the direct fission occurs only for subbarrier excitation energies and only through discrete channels, that is,

$$T_{dir}(EJ\pi) = \sum_{K \leqslant J} T_{dir}(EKJ\pi), \quad (19)$$

while the absorption in the isomeric well occurs through all fission channels.

In the full K-mixing approximation, all the discrete channels with the same $J\pi$ contribute irrespective of their K value to the total absorption coefficient. The continuum fission channels contribute at higher energies, where the class II states are completely damped and the entire flux transmitted through the inner barrier is absorbed in the isomeric well; thus,

$$T_{abs}(EJ\pi) = \sum_{K \leqslant J} T_{abs}(EKJ\pi)$$
$$+ \int_{E_{cA}}^{\infty} \frac{\rho_A(\varepsilon J\pi)d\varepsilon}{1 + \exp\left[-\frac{2\pi}{\hbar\omega_A}(E - V_A - \varepsilon)\right]}. \quad (20)$$

B. Decay probabilities

Usually the fissioning nucleus is populated mainly in class I states. From these states, it decays by particle or γ emission or by direct fission, or it can change shape by a transition to a class II state (absorption in the isomeric well). The fraction absorbed in the isomeric well can decay by direct fission through the outer humps, by transition to the isomeric state, or by another change of shape (coming back to a class I state). The fraction returned to the class I state is divided again, and the process continues indefinitely. The formulas for the decay probabilities which take into account the infinite series of transitions, hence guarantee the flux conservation, have been derived in [11,12] by generalizing the procedure outlined in [1]. The lengthy derivation is shown in the Appendix B. As a result, we obtain the total fission probability

$$P_f = P_{dir} + P_{ind} = \frac{T_{dir}}{T_{dir} + \sum_d T_d}\left(1 - \frac{1}{a}\right) + \frac{1}{a}, \quad (21)$$

where

$$a = \left[1 + b^2 + 2b \coth\left(\frac{T_A + T_{BC}}{2}\right)\right]^{1/2}, \quad (22)$$

$$b = \frac{\left(T_{dir} + \sum_d T_d\right)(T_A + T_{BC})}{T_{abs}T_{BC}}. \quad (23)$$

The general expression (21) is valid for partial damping of class II vibrational states and can be applied at any excitation energy below or above the fission barrier. It shows that from the flux destined to fission by direct transmission across the barrier, part $1/a$ is taken out and reemitted into the fission channel after being absorbed in the isomeric well.

At very low excitation energies, where the class II vibrational states preserve their individuality, fission proceeds entirely by direct transmission across the barrier and the second term $P_{ind} = 1/a$ in Eq. (21) disappears. In the opposite case, that of complete damping, the entire flux transmitted through the inner hump is absorbed in the isomeric well, γ decay on the isomeric state becomes negligible, and the well-known expression for the decay probabilities is obtained,

$$P_k = \frac{T_k}{T_f + \sum_d T_d} \qquad k = f, d, \quad (24)$$

with the fission coefficient T_f given by

$$T_f = \frac{T_A T_{BC}}{T_A + T_{BC}}. \quad (25)$$

The cross sections for fission and for competing channels are calculated using the relation

$$\sigma_k(E) = \sum_{J^\pi} \sigma(EJ\pi)P_k(EJ\pi) \qquad k = f, d, \quad (26)$$

where $\sigma(EJ\pi)$ is the fissioning nucleus formation cross section, and the decay probabilities $P_k(EJ\pi)$ are given by Eqs. (B16) and (B17) in Appendix B for fission and other outgoing channels correspondingly.

III. ^{232}Th AND ^{231}Pa NEUTRON-INDUCED FISSION

The capability of the optical model for fission, presented in the previous section, to accurately describe fission cross sections and provide fission barrier parameters for light actinides, was tested on ^{232}Th(n, f) and ^{231}Pa(n, f) reactions. A formalism based on this model has been recently implemented in the EMPIRE-2.19 nuclear reaction code [22,23]. Using this code, a full evaluation of neutron-induced reactions on the ^{232}Th nucleus from 1 keV up to 60 MeV has been carried out [24] and will be published in a separate paper. To ensure a reliable fission cross section analysis, a very good description of all available experimental data was obtained, as can be seen from Figs. 3–6, corresponding to the energy range below 6 MeV studied in this work. A similar evaluation for ^{231}Pa is under way. In these calculations, the direct interaction cross sections and transmission coefficients for the incident channel on ^{232}Th and ^{231}Pa were obtained from the dispersive coupled-channel optical models given in Refs. [49] and [50], respectively. The coupled-channel ECIS03 code [51,52] incorporated into the EMPIRE-2.19 system [22] was used for optical model calculations. Preequilibrium emission is negligible below 6 MeV. Hauser-Feshbach (HF) [53] and Hofmann-Richert-Tepel-Weidenmüller (HRTW) [54] versions of the statistical model were used for the compound nucleus cross section calculations. Both approaches include decay probabilities deduced in the optical model for fission
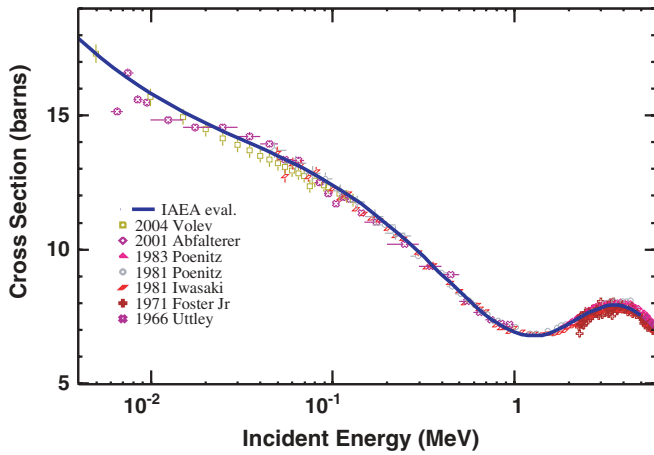
FIG. 3. (Color online) Total cross section for interaction of neutrons on ^{232}Th. Experimental data were taken from EXFOR [25–31].

presented here and account for the multiple-particle emission and the full γ cascade.

Let us focus on the calculation of the first-chance fission in the two nuclei under study. A complete study would require the analysis of (i) the fission fragment angular distributions to extract information about the K^π bandheads and (ii) the gross and fine resonant structure of the fission cross section to extract information about the excitation energies of the vibrational states, moments of inertia, and decoupling parameters. For evaluation purposes, treatment of the fission channel should use a minimum number of input parameters, but at the same time, it should be sophisticated enough to describe the experimental data with the accuracy required by applications. Therefore, we focus on reproducing the gross vibrational resonant structure of the fission cross section, without attempting to describe the fine structure related to rotational levels. Crucial to this type of calculation are, beside the fission model itself, the set of fission barrier parameters consisting of (i) heights and widths of the parabolas describing the fundamental barriers, (ii) discrete transition states at saddle
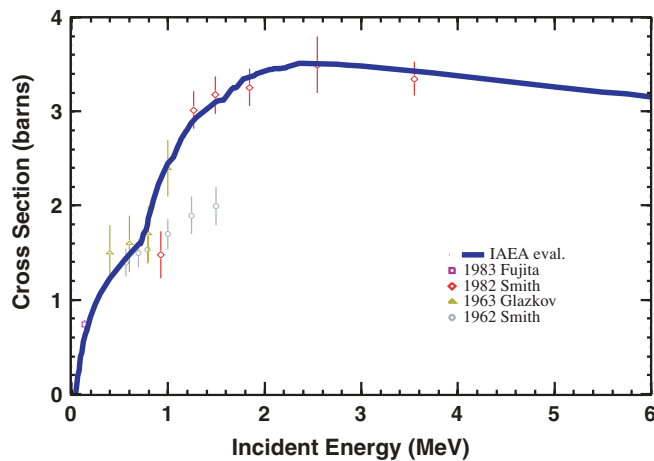

FIG. 4. (Color online) Nonelastic cross section of ^{232}Th. Experimental data were taken from EXFOR [32–35].
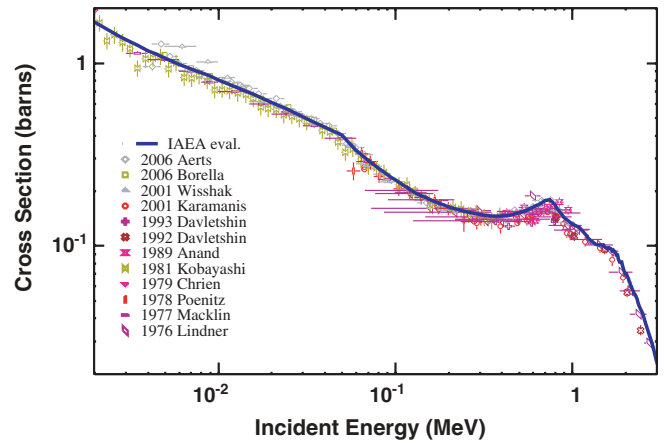

FIG. 5. (Color online) Neutron capture cross section of ^{232}Th. Experimental data were taken from EXFOR [36–47].

points and in intermediate wells, and (iii) level densities at saddle points. For the present study, these parameters have been empirically determined from the analysis of the measured fission cross sections, considering values reported in the literature and the overall fit of the available experimental data for competing channels.

A. ^{232}Th(n, f) reaction

The analysis of the experimental data for ^{232}Th first-chance fission cross section (Figs. 7 and 8) reveals the following features:

(i) A resonant structure above the fission threshold indicating the existence of a third shallow well accommodating undamped hyperdeformed vibrational states.

(ii) A first change of slope around the neutron incident energy of 1.1 MeV, suggesting a height of the inner barrier of 5.9 ± 0.2 MeV (the neutron separation energy in ^{233}Th is 4.78 MeV).
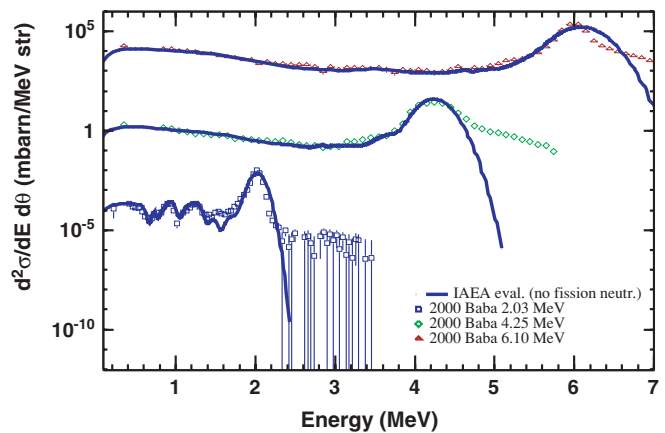

FIG. 6. (Color online) Neutron emission cross sections at 30° for 2.03, 4.25, and 6.1 MeV incident neutron energy on ^{232}Th. Experimental data measured by Baba *et al.* [48]. 4.25 and 6.1 MeV plots are scaled by 10^3 and 10^6 factors, respectively. Fission neutrons' contribution is not shown.
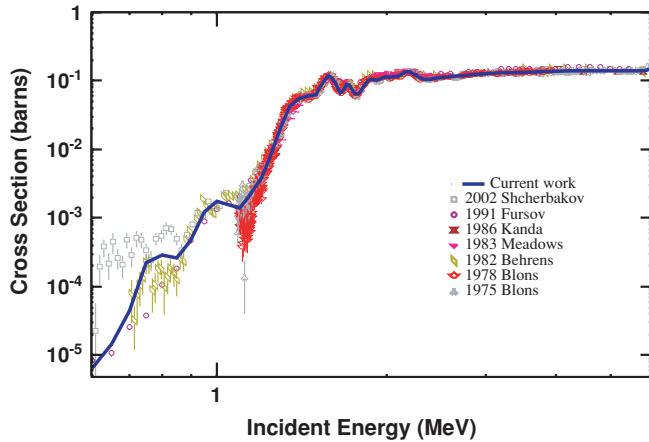
FIG. 7. (Color online) Neutron-induced fission cross section of ^{232}Th from 0.5 to 5.9 MeV. Experimental data were taken from EXFOR [55–61].

FIG. 8. (Color online) Neutron-induced fission cross section of ^{232}Th near the fission threshold. Experimental data were taken from EXFOR [55–61].

(iii) Wide resonances below 1.1 MeV which could be associated with partially damped vibrational states in the second well.

(iv) A fission threshold around the neutron incident energy of 1.5 MeV, suggesting a height of the outer barriers of 6.3 ± 0.2 MeV.

(v) The positions of the resonances assumed to be related to the class II and class III states and the rising smooth part between them (from 1.1 to 1.5 MeV) indicating that the excitation energy ranges of the vibrational states in the two wells do not overlap (see Appendix A and region IV in Fig. 2).

The best description of the experimental data was obtained by using fission barrier parameters in perfect agreement with these assumptions (see Table I). The inner barrier parameters ($V_A = 5.82$ MeV, $\hbar\omega_A = 1.00$ MeV) are supported by some recent calculations [5] and differ from earlier predictions [2,15], indicating a lower and wider inner hump. The parameters of the second well were deduced from the position of the wide resonances at low energies related to the class II vibrational states. The experimental data are scarce in this energy range, so we adopted values typical of actinides: $V_{II} = 2.12$ MeV for the depth (defined with respect to the ground state) and $\hbar\omega_{II} = 1.00$ MeV for the width. For the heights of the second and third hump, the values of $V_B = 6.35$ MeV and $V_C = 6.45$ MeV were adopted. The widths of these humps ($\hbar\omega_{B,C} = 1.30$ MeV) were deduced from the slope of the fission barrier at excitation energies above the inner barrier. The parameters of the third well represent a controversial subject: early calculations predicted a rather shallow well with a depth of 0.2–0.5 MeV accommodating undamped class III
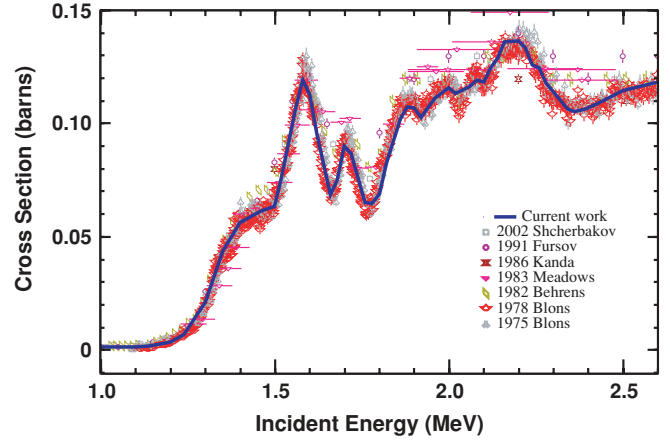
vibrational states, while more recent experimental [62] and theoretical [63] studies support the idea of a much deeper well with a depth of up to 3 MeV, which might require a partial damping. Independently of the depth of the third well, however, we expect in general that class III resonances should be less damped than class II resonances, since the main microscopic source of damping is the coupling to class I compound states. This coupling is much less likely in the third well, where the nucleus is reflection asymmetric and strongly elongated, than in the second well, where the nucleus is reflection symmetric and less deformed, and thus closer to the characteristics of the first well. The fact that the present formalism does not allow for the damping of class III vibrational states might affect the shape, but not the positions of the resonances. Our calculations show that a deep third well gives rise to a resonant structure, especially at energies below the threshold, while a shallower well produces resonances in the plateau region. The measured thorium fission cross section would indicate a shallow third well, although resonances below 1.1 MeV could also be related to partially damped class III vibrational states in a deeper third well. The best description of the data was obtained using the depth of around 0.7 MeV ($V_{III} = 5.65$ MeV) and the width $\hbar\omega_{III} = 1.00$ MeV. One can notice that the bottom of the third well is close to the top of the first hump, indicating that the positions of the class III vibrational states correspond to excitation energies for which the class II vibrational states are almost completely damped. Therefore, there is no interference among the resonances due to the states in the two wells, confirming our initial hypothesis.

The parameters of the barriers associated with the discrete transition states presented in Table II have been deduced from

TABLE I. Parameters of fundamental triple-humped fission barrier (in MeV) for ^{233}Th and ^{232}Pa.

Compound nucleus	V_A	$\hbar\omega_A$	V_{II}	$\hbar\omega_{II}$	V_B	$\hbar\omega_B$	V_{III}	$\hbar\omega_{III}$	V_C	$\hbar\omega_C$
^{233}Th	5.82	1.00	2.12	1.00	6.35	1.30	5.65	1.00	6.45	1.30
^{232}Pa	5.92	0.50	1.90	1.00	6.30	1.20	5.40	1.00	6.34	1.10

TABLE II. Transition bandheads (keV) for ^{233}Th.

K^π	ϵ_A	ϵ_{II}	ϵ_B	ϵ_{III}	ϵ_C	K^π	ϵ_A	ϵ_{II}	ϵ_B	ϵ_{III}	ϵ_C
$1/2^+$	200	100	100	180	200	$1/2^-$	200	300	100	200	300
$1/2^+$	300	500	500	450	600	$1/2^-$	300	800	400	500	350
$1/2^+$	400	700	600	750	650	$1/2^-$	500	850	500	800	600
$1/2^+$	500	900	650	800	700	$1/2^-$	700	900	550	850	650
$3/2^+$	200	250	300	300	500	$3/2^-$	200	650	300	300	350
$3/2^+$	300	760	600	550	600	$3/2^-$	300	700	600	600	650
$5/2^+$	0	0	0	0	0	$5/2^-$	100	180	100	50	0
$5/2^+$	250	800	500	650	600	$5/2^-$	300	850	600	700	600

fit, considering also the asymmetry of the third well. For the widths, very similar values to those of the fundamental barrier have been used, therefore they are not included in the table. The strength of the imaginary potential in the isomeric well was chosen to fit the width of the wide resonances at subbarrier energies (0.8, 1.0 MeV) and to assure a complete damping close to the top of the inner barrier.

The contribution of the continuum to the fission coefficients is calculated using an equivalent double-humped fission barrier (see Sec. II and Fig. 1). The parameters of the equivalent outer barrier are $V_{eq} = 6.64$ MeV and $\hbar\omega_{eq} = 0.75$ MeV. For the description of the continuous part of the fission transition spectra the same level density formalism as for the normal states was used. It is based on the superfluid model below the critical excitation and the Fermi gas model above, and includes deformation-dependent collective effects [22]. The shell correction, pairing, and asymptotic value of the level density parameter at each saddle have been calculated following RIPL-2 recommendations [64]. For the studied nuclei, the impact of the level density parameters on the description of resonant structure near the fission threshold is relatively small.

As demonstrated in Figs. 7 and 8, the optical model for fission with the barrier parameters discussed above provides a very good description of the available experimental data of the

first-chance fission of ^{232}Th. It is worthwhile to mention that the optical model for fission was also shown to give a good description of photon-induced fission on ^{232}Th as can be seen in Fig. 8 of Ref. [23], where preliminary results of the present work were presented.

B. ^{231}Pa(n, f) reaction

The measured neutron-induced fission cross section of the ^{231}Pa nucleus has a complicated structure (see Figs. 9 and 10). Analyzing it we can notice the following features concerning the fission barrier parameters:

(i) As in the ^{232}Th case, a pronounced resonant structure above the fission threshold indicates a triple-humped barrier.

(ii) Unlike the ^{232}Th case, a superposition of wide ($E_n = 0.185, 0.315$ MeV) and sharp ($E_n = 0.155, 0.173, 0.370$ MeV) resonances in the subthreshold region indicates a coexistence of class II and III vibrational states in this excitation energy range (see Appendix A and region III in Fig. 2).

(iii) There is no obvious change of slope, but above 0.4 MeV neutron incident energy, there are no more wide resonances (presumptively related to the partially damped class II vibrational states), meaning that the height of
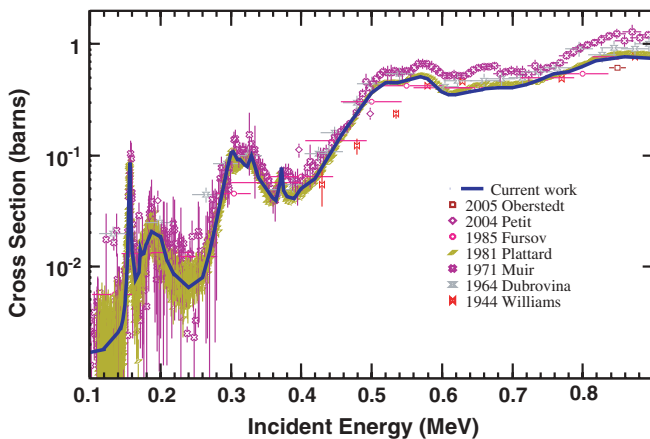

FIG. 9. (Color online) Neutron-induced fission cross section of ^{231}Pa from 0.1 to 5 MeV. Experimental data were taken from references [65–71].
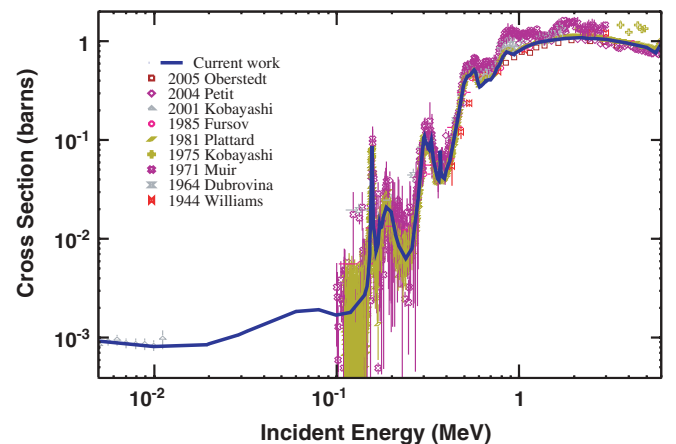

FIG. 10. (Color online) Neutron-induced fission cross section of ^{231}Pa. Experimental data were taken from references [65–73].

TABLE III. Transition bandheads (keV) for ^{232}Pa.

K^π	ϵ_A	ϵ_{II}	ϵ_B	ϵ_{III}	ϵ_C	K^π	ϵ_A	ϵ_{II}	ϵ_B	ϵ_{III}	ϵ_C
0^+	20	100	80	80	100	0^-	20	30	100	70	100
0^+	80	200	180	100	200	0^-	100	100	120	100	150
0^+	100	400	200	250	250	0^-	120	150	500	200	400
1^+	10	30	50	20	50	1^-	100	100	50	50	150
1^+	100	150	80	40	100	1^-	70	250	100	90	150
1^+	150	160	100	250	100	1^-	100	400	120	200	250
1^+	160	300	170	500	200	1^-	130	480	200	500	200
1^+	200	400	200	650	200	1^-	300	550	220	700	300
2^+	10	60	30	10	30	2^-	0	0	0	0	0
2^+	50	130	80	50	100	2^-	40	40	60	50	150
2^+	100	210	100	160	150	2^-	90	150	100	120	100
2^+	150	300	150	300	200	2^-	200	200	150	320	250
2^+	200	350	300	420	400	2^-	220	250	300	370	350
3^+	100	260	400	550	400	3^-	200	400	500	520	450
3^+	130	300	450	600	400	3^-	300	480	550	580	500
3^+	210	400	500	650	600	3^-	400	550	600	700	600

the inner barrier would be 5.9 ± 0.2 MeV (the neutron separation energy in ^{232}Pa is 5.55 MeV).

(iv) The fission threshold around 0.5 MeV neutron incident energy suggests heights of the outer barriers of 6.1 ± 0.2 MeV.

(v) The sharp resonances below the threshold, assumed to be related to class III vibrational states, would indicate a deeper third well.

Again our calculations are fully consistent with these assumptions. The best description of the fission cross section was obtained when using for the fundamental barrier the parameters in Table I. They are similar to those obtained for thorium, with two exceptions: the smaller width of the first hump ($\hbar\omega_A = 0.5$ MeV) needed to reproduce the relatively low value of the protoactinium fission cross section at low energies and, as expected, the lower value of the third well bottom ($V_{III} = 5.40$ MeV) allowing the description of the sharp resonances at subthreshold energies.

The parameters of the barriers associated with discrete transition states presented in Table III have been deduced to fit the resonances. The calculations show that in the protactinium case, resonances produced by vibrational states in the isomeric well are strongly influenced by positions of corresponding transition states in the third well. This could explain why the fissioning compound nucleus ^{232}Pa has such spectacular resonant structure as observed in Fig. 10, which is partially related to the vibrational states in the isomeric well, despite the fact that it is doubly odd. It is known that the neutron-induced fission cross section of the odd-even targets [e.g., ^{241}Am(n, f) cross section] is usually smooth, without any resonant structure. This is related to the complete damping of the vibrational states in the isomeric well, explained by the small distance among the class II vibrational and nonvibrational states compared to their widths, specific for doubly-odd nuclei. The atypical behavior of the ^{231}Pa(n, f) cross section could be explained by the

coexistence of the second and third wells in the fission barrier. Therefore, the penetrability through the class II vibrational states is being "triggered" by the class III vibrational states. Of course, the possibility that all the resonances are related to class III vibrational states cannot be completely ruled out; further studies of the fission transition state spectra are warranted.

The strength of the imaginary potential in the isomeric well was chosen to fit the width of the wide resonances at subbarrier energies and to ensure a complete damping close to the top of the inner barrier. The contribution of the transition states in continuum to the fission coefficients was calculated following the same procedure as for ^{232}Th. The parameters of the equivalent outer barrier used in calculations are $V_{eq} = 6.05$ MeV, $\hbar\omega_{eq} = 0.50$ MeV.

A good agreement of the ^{231}Pa(n, f) calculated cross section with the experimental data is demonstrated in Figs. 9 and 10. Further refinement of the calculation will be possible after the evaluation of competing particle emission channels is finished.

IV. CONCLUSIONS

A model to describe fission in light actinides, which takes into account transmission through a triple-humped fission barrier with absorption, has been developed. This formalism is capable of interpreting complex structure in the light actinide fission cross section in a wide energy range. It can be applied at sub- and overbarrier energies for neutron- and photon-induced fission. The fission probability derived in the WKB approximation within optical model for fission has been incorporated into the statistical model of nuclear reactions. The complex resonance structure in the first-chance neutron-induced fission cross sections of ^{232}Th and ^{231}Pa nuclei has been well reproduced by the proposed model. Consistent sets of parameters describing the triple-humped fission barriers of ^{233}Th and ^{232}Pa have been obtained. A

0.7 (0.9) MeV shallow third well is obtained for thorium (protactinium) allowing us to neglect damping in this well. Calculations confirm the attribution of the gross resonant structure in the fission probability of these light actinides to a combination of partially damped vibrational states in the second well and undamped vibrational states in the tertiary well of the fission barriers.

We are aware that (n, f) cross sections alone do not permit the unique determination of the fission barrier parameters of superdeformed and hyperdeformed states. Additional experimental data, such as angular distributions of fission fragments, would be useful. It is our intention to analyze them, once they are available, using a more refined theoretical model, including direct evaluation of fission barriers [74] as well as theoretical parametrization of transition states by means of a suitable collective model of nuclear structure.

APPENDIX A

The general relations for the direct transmission coefficient [Eq. (10)] and for the absorption coefficient in the isomeric well [Eq. (14)] take the following particular forms in the excitation energy regions indicated in Fig. 2:

  (i) Region I corresponds to excitation energies lower than the isomeric well. The fission coefficient T_f is calculated by numerical integration as the transmission coefficient through the whole fission barrier.

 (ii) Region II corresponds to excitation energies higher than the isomeric well and lower than the outer well. The fission coefficient is calculated as in the case of a double-humped barrier, whose WKB formulas were first derived in Ref. [16] for a real barrier and in Ref. [15] for a more general case of a complex potential in the intermediate well, that is,

$$T_{\mathrm{dir}} = \frac{T_A T_B}{e^{2\delta} + 2(1 - T_A)^{1/2}(1 - T_B)^{1/2}\cos(2\nu_1) + (1 - T_A)(1 - T_B)e^{-2\delta}}, \tag{A1}$$

$$T_{\mathrm{refl}} = \frac{T_{\mathrm{dir}}}{T_A T_B}[e^{2\delta}(1 - T_A) + e^{-2\delta}(1 - T_B) + 2(1 - T_A)^{1/2}(1 - T_B)^{1/2}\cos(2\nu_1)], \tag{A2}$$

$$T_{\mathrm{abs}} = 1 - T_{\mathrm{dir}} - T_{\mathrm{refl}} = T_{\mathrm{dir}}\frac{e^{2\delta} - (1 - T_B)e^{-2\delta} - T_B}{T_B}. \tag{A3}$$

In the present case, T_B is replaced with the transmission through the outer humps T_{BC}, calculated by numerical integration through the outer barriers B and C.

(iii) Region III corresponds to excitation energies higher than the outer well and lower than the first hump. In this energy range, class II and class III states coexist. The direct and absorption coefficients are calculated using the relations (10) and (14). This region is key to the successful description of neutron-induced fission on ^{231}Pa.

(iv) Region IV appears when the height of the first hump is lower than the outer well, and the excitation energy is higher than the height of the first hump. This case corresponds to a two-humped barrier with full absorption in the isomeric well ($T_{\mathrm{abs}} \rightarrow T_A \rightarrow 1$, $T_{\mathrm{dir}} \rightarrow 0$, $T_{\mathrm{refl}} \rightarrow 0$) and the transmission through the outer humps T_{BC}, calculated numerically. It is worthwhile to point out the difference between the transmission coefficient through the barrier $T = T_{\mathrm{refl}} + T_{\mathrm{dir}} + T_{\mathrm{abs}} \rightarrow 1$ and the fission coefficient (4), which at overbarrier energies, where $T_{\gamma \mathrm{II}} \rightarrow 0$ and the full damping limit is reached, becomes

$$T_f = \frac{T_A T_{BC}}{T_A + T_{BC}} \tag{A4}$$

and tends to 1/2.

 (v) Region V is similar to Region IV ($T_{\mathrm{abs}} \rightarrow T_A$, $T_{\mathrm{dir}} \rightarrow 0$) except that T_{BC} refers to the direct transmission (without absorption) through the second and third humps, which is

$$T_{BC} = \frac{T_B T_C}{1 + 2[(1 - T_B)^{1/2}(1 - T_C)^{1/2}\cos(2\nu_2) + (1 - T_B)(1 - T_C)]}. \tag{A5}$$

(vi) Region VI corresponds to excitation energies higher than the lowest of humps 2 and 3. At these energies, class III vibrational states become completely damped; therefore, the direct transmission through the outer humps disappears $T_{BC} \to 0$, the transmission through these humps occurring only through states in continuum [see Eq. (18)]. The limits of the absorption coefficient in the isomeric well and of the direct transmission coefficient through the entire well remain: $T_{abs} \to T_A$ and $T_{dir} \to 0$.

APPENDIX B

To define the decay probabilities of the actinide nuclei with multihumped fission barriers and an imaginary potential in the isomeric well, a unitary initial flux populating class I states was considered (for the sake of simplicity the dependence of all quantities on $EJ\pi$ will be not written explicitly). A part of this flux (N_d^0) decays by competing processes (particle or γ emission), a part (N_{refl}^0) is reflected, a part (N_{dir}^0) is transmitted directly through the barrier (undergoes direct fission), and a part (N_{abs}^0) changes shape by a transition to a class II state (absorption in the isomeric well):

$$1 = \sum_d N_d^0 + N_{refl}^0 + N_{dir}^0 + N_{abs}^0. \tag{B1}$$

These fractions of the initial flux are expressed in terms of the corresponding transmission coefficients as

$$N_i^0 = \frac{T_i}{\sum_d T_d + T_{refl} + T_{dir} + T_{abs}} = \frac{T_i}{\sum_m T_m}, \tag{B2}$$

where $i, m = d$, refl, dir, abs. The fraction absorbed in the isomeric well can be transmitted directly through the outer humps (indirect fission), can decay γ to the isomeric state, or can rechange shape (coming back to a class I state by penetrating the inner hump backward). Neglecting the γ decay to the isomeric state, it reads

$$N_{abs}^0 = N_A^0 + N_{BC}^0 , \tag{B3}$$

where

$$N_j^0 = N_{abs}^0 \frac{T_j}{T_A + T_{BC}} = N_{abs}^0 \frac{T_j}{\sum_n T_n} = \frac{T_{abs}}{\sum_m T_m} \cdot \frac{T_j}{\sum_n T_n}, \tag{B4}$$

where $i, m = d$, refl, dir, abs; $j, n = A, BC$. Now we can iterate, so the fraction returned to class I states is partitioned again (as was done for the initial flux) into

$$N_A^0 + N_{refl}^0 = \sum_d N_d^1 + N_{refl}^1 + N_{dir}^1 + N_{abs}^1, \tag{B5}$$

$$N_i^1 = \left(N_A^0 + N_{refl}^0\right) \frac{T_i}{\sum_m T_m}$$
$$= \left(\frac{T_{abs}}{\sum_m T_m} \frac{T_A}{\sum_n T_n} + \frac{T_{refl}}{\sum_m T_m}\right) \frac{T_i}{\sum_m T_m}, \tag{B6}$$

where $i, m = d$, refl, dir, abs; $n = A, BC$.

$$N_{abs}^1 = N_A^1 + N_{BC}^1, \tag{B7}$$

$$N_j^1 = N_{abs}^1 \frac{T_j}{\sum_n T_n}$$
$$= \left[\frac{T_{abs}}{\sum_m T_m} \frac{T_A}{\sum_n T_n} + \frac{T_{refl}}{\sum_m T_m}\right] \frac{T_{abs}}{\sum_m T_m} \frac{T_j}{\sum_n T_n}, \tag{B8}$$

where $m = d$, refl, dir, abs; $j, n = A, BC$, and the process continues indefinitely. The total flux fractions decaying in different channels from the first and second well represent the sum of infinite series

$$N_i = \sum_{k=0}^{\infty} N_i^k = \frac{T_i}{\sum_m T_m} \sum_{k=0}^{\infty} \left(\frac{T_{abs}}{\sum_m T_m} \frac{T_A}{\sum_n T_n} + \frac{T_{refl}}{\sum_m T_m}\right)^k$$
$$= \frac{T_i}{\sum_m T_m} \left[1 - \frac{1}{\sum_m T_m} \left(\frac{T_{abs} T_A}{\sum_n T_n} + T_{refl}\right)\right]^{-1} \tag{B9}$$

where $i, m = d$, refl, dir, abs; $n = A, BC$.

$$N_j = \sum_{k=0}^{\infty} N_j^k = \frac{T_j}{\sum_n T_n} \frac{T_{abs}}{\sum_m T_m}$$
$$\times \sum_{k=0}^{\infty} \left(\frac{T_{abs}}{\sum_m T_m} \frac{T_A}{\sum_n T_n} + \frac{T_{refl}}{\sum_m T_m}\right)^k$$
$$= \frac{T_j}{\sum_n T_n} \frac{T_{abs}}{\sum_m T_m} \left[1 - \frac{1}{\sum_m T_m} \left(\frac{T_{abs} T_A}{\sum_n T_n} + T_{refl}\right)\right]^{-1}, \tag{B10}$$

where $m = d$, dir, abs; $j, n = A, BC, \gamma_{II}$. The quantities needed for the decay probability calculations are N_{dir}, N_{BC}, and N_d, for which the above formulas become

$$N_{dir} = \frac{T_{dir}}{T_{dir} + \sum_{d'} T_{d'} + T_{abs} T_{BC}/(T_A + T_{BC})},$$

$$N_{BC} = \frac{T_{abs}}{T_{dir} + \sum_{d'} T_{d'} + T_{abs} T_{BC}/(T_A + T_{BC})} \frac{T_{BC}}{T_A + T_{BC}},$$

$$N_d = \frac{T_d}{T_{dir} + \sum_{d'} T_{d'} + T_{abs} T_{BC}/(T_A + T_{BC})}.$$

The coupling of class I and class II states is considered according to [10] by multiplying T_{abs} with the weight function

$$f(x, \Gamma_{cII}, D_{II}) = \frac{\sinh(2\pi \Gamma_{cII}/D_{II})}{\cosh(2\pi \Gamma_{cII}/D_{II}) - \cos(2\pi x/D_{II})}, \tag{B11}$$

where $x = E - E_0$ is the difference between the excitation energy and the centroid excitation energy of the class II level, D_{II} is the distance between the class II levels in the picket fence approximation, and Γ_{cII} represents the decay width of

the class II levels expressed in terms of the transmission coefficients through the humps and of the γ decay in the second well: $2\pi\Gamma_{c\mathrm{II}}/D_{\mathrm{II}} = T_A + T_{BC}$.

Averaging over a class II resonance, the following expressions for the direct and indirect fission probabilities are obtained:

$$P_{\mathrm{dir}} = \frac{1}{D_{\mathrm{II}}} \int_{-D_{\mathrm{II}}/2}^{D_{\mathrm{II}}/2} N_{\mathrm{dir}} dx = \frac{T_{\mathrm{dir}}}{T_{\mathrm{dir}} + \sum_{d'} T_{d'}} \left(1 - \frac{1}{a}\right),$$ (B12)

$$P_{\mathrm{ind}} = \frac{1}{D_{\mathrm{II}}} \int_{-D_{\mathrm{II}}/2}^{D_{\mathrm{II}}/2} N_{BC} dx = \frac{1}{a},$$ (B13)

where

$$a = \left[1 + b^2 + 2b \coth\left(\frac{T_A + T_{BC}}{2}\right)\right]^{1/2},$$ (B14)

$$b = \frac{\left(T_{\mathrm{dir}} + \sum_{d'} T_{d'}\right)(T_A + T_{BC})}{T_{\mathrm{abs}} T_{BC}}.$$ (B15)

The total fission probability reads

$$P_f = P_{\mathrm{dir}} + P_{\mathrm{ind}} = \frac{T_{\mathrm{dir}}}{T_{\mathrm{dir}} + \sum_{d'} T_{d'}} \left(1 - \frac{1}{a}\right) + \frac{1}{a},$$ (B16)

and the total decay probabilities for the competing channels P_d read

$$P_d = \frac{1}{D_{\mathrm{II}}} \int_{-D_{\mathrm{II}}/2}^{D_{\mathrm{II}}/2} N_d dx = \frac{T_d}{T_{\mathrm{dir}} + \sum_{d'} T_{d'}} \left(1 - \frac{1}{a}\right).$$ (B17)

These relations can be applied in the case of the double-humped fission barrier by replacing the direct transmission coefficient through the outer barriers T_{BC} with the transmission coefficient across the outer barrier T_B.

[1] S. Bjornholm and J. E. Lynn, Rev. Mod. Phys. **52**, 725 (1980).
[2] J. Blons, C. Mazur, D. Paya, M. Ribrag, and H. Weigmann (EXFOR 21656), Nucl. Phys. **A414**, 1 (1984).
[3] B. S. Bhandari, Phys. Rev. C **42**, 1443 (1990).
[4] A. Krasznahorkay, A. Habs, M. Hunyadi, D. Gassmann, M. Csatlós, Y. Eisermann, T. Faestermann, G. Graw, J. Gulyás, R. Hertenberger, H. J. Maier, Z. Máté, A. Metz, J. Ott, P. Thirolf, and S. Y. van der Werf, Phys. Lett. **B461**, 15 (1999).
[5] P. G. Thirolf and D. Habs, Prog. Part. Nucl. Phys. **49**, 325 (2002).
[6] M. J. Lopéz Jiménez, B. Morillon, and P. Romain, Ann. Nucl. Energy **32**, 195 (2005).
[7] A. Trkov, Technical report INDC(NDS)-447, IAEA, Vienna, 2003. Available online at http://www-nds.iaea.org/reports/indc-nds-447.pdf
[8] V. M. Maslov, Nucl. Phys. **A757**, 390 (2005).
[9] Y. Han and Z. Zhang, Nucl. Phys. **A753**, 53 (2005).
[10] B. B. Back, O. Hansen, H. C. Britt, and J. D. Garrett, Phys. Rev. C **9**, 1924 (1974).
[11] M. Sin and G. Vladuca, in *Proceedings of the International Conference on Nuclear Data for Science and Technology, Trieste, May 19–24, 1997*, edited by G. Reffo, A. Ventura and C. Grandi (Italian Physical Society, Bologna, 1997); Conference Proceedings **59**, Part I, p. 976.
[12] M. Sin, G. Vladuca, and C. Negoita, Ann. Nucl. Energy **27**, 995 (2000).
[13] N. Froman and P. O. Froman, *JWKB Approximation, Contributions to the Theory* (North-Holland, Amsterdam, 1965).
[14] S. G. Nilsson, J. R. Nix, A. Sobiczewski, Z. Szymanski, S. Wycech, C. Gustafson, and P. Moller, Nucl. Phys. **A115**, 545 (1968).
[15] B. S. Bhandari, Phys. Rev. C **19**, 1820 (1979).
[16] N. Froman and O. Dammert, Nucl. Phys. **A147**, 627 (1970).
[17] T. Martinelli, E. Menapace, and A. Ventura, Lett. Nuovo Cimento **20**, 267 (1977).
[18] J. C. P. Miller, in *Handbook of mathematical functions*, Ch. 19, p. 685, edited by M. Abramowitz and I. A. Stegun (Dover, New York, 1972).
[19] G. Maino, E. Menapace, and A. Ventura, J. Comput. Phys. **40**, 294 (1981).
[20] R. C. Sharma and J. N. Leboeuf, Phys. Rev. C **14**, 2340 (1976).
[21] T. Martinelli, E. Menapace, and A. Ventura, CNEN Technical Report RT/FI(78)7, Bologna, 1978.
[22] M. Herman, P. Obložinský, R. Capote, M. Sin, A. Trkov, A. Ventura, and V. Zerkin, in *Proceedings of the International Conference on Nuclear Data for Science and Technology, 27 September–1 October 2004*, Santa Fé, N. M.; AIP Conf. Proc. **769** (AIP, New York, 2005), p. 1184. Code distributed online at http://www.nndc.bnl.gov/empire219/index.html
[23] M. Sin, R. Capote, M. Herman, P. Obložinský, A. Ventura, and A. Trkov, in *Proceedings of the International Conference on Nuclear Data for Science and Technology, 27 September–1 October, 2004*, Santa Fé, N. M.; AIP Conf. Proc. **769** (AIP, New York, 2005), p. 1249.
[24] R. Capote, M. Sin, and A. Trkov (in preparation).
[25] K. Volev, N. Koyumdjieva, A. Brusegan, A. Borella, P. Siegler, N. Janeva, A. Lukyanov, L. Leal, and P. Schillebeeckx, in *Proceedings of the International Conference on Nuclear Data for Science and Technology, 27 September–1 October, 2004*, Santa Fé, N. M.; AIP Conf. Proc. **769** (AIP, New York, 2005), p. 87.
[26] W. P. Abfalterer, F. B. Bateman, F. S. Dietrich, R. W. Finlay, R. C. Haight, and G. L. Morgan (EXFOR 13753), Phys. Rev. C **63**, 044608 (2001).
[27] W. P. Poenitz and J. F. Whalen (EXFOR 12853). Technical report ANL-NDM-80, Argonne National Laboratory, 1983.
[28] W. P. Poenitz, J. F. Whalen, and A. B. Smith (EXFOR 10935), Nucl. Sci. Eng. **78**, 333 (1981).
[29] T. Iwasaki, M. Baba, K. Hattori, K. Kanda, S. Chiba, K. Kanoda, and N. Hirakawa (EXFOR 21767), In *Contribution to the Specialists' Meeting on fast neutron scattering on actinide nuclei, Japan, 1981*.
[30] D. G. Foster Jr., and D. W. Glasgow (EXFOR 10047), Phys. Rev. C **3**, 576 (1971).
[31] C. A. Uttley, C. M. Newstead, and K. M. Diment (EXFOR 21088), Technical report AERE-PR/NP-9, p.5; AERE-PR/NP-10, p. 8, A.E.R.E. Harwell, U.K., 1966.
[32] Y. Fujita, T. Ohsawa, R. M. Bugger, D. M. Alger, and W. H. Miller. (EXFOR 12858), J. Nucl. Sci. Technol. **20**, 983 (1983).
[33] A. B. Smith and P. T. Guenther (*EXFOR 12742*), Technical report ANL-NDM-63, Argonne National Laboratory, 1982.

[34] N. P. Glazkov (EXFOR 40662), At. Energ. **15**, 416 (1963).

[35] A. B. Smith (EXFOR 12277), Phys. Rev. **126**, 718 (1962).

[36] G. Aerts *et al.* (nTOF Collaboration), Phys. Rev. C **73**, 054610 (2006).

[37] A. Borella, K. Volev, A. Brusegan, P. Schillebeeckx, F. Corvi, N. Janeva, N. Koyumdjieva, and A. A. Lukyanov (EXFOR 22875), Nucl. Sci. Eng. **152**, 1 (2006).

[38] K. Wisshak, F. Voss, and F. Kaeppeler. (EXFOR 22654), Nucl. Sci. Eng. **137**, 183 (2001).

[39] D. Karamanis, M. Petit, S. Andriamonje, G. Barreau, M. Bercion, A. Billebaud, B. Blank, S. Chajkowski, V. Lacoste, C. Marchand, R. Del Moral, J. Giovinazzo, L. Perrot, M. Pravikoff, and J. C. Tomas (EXFOR 22663), Nucl. Sci. Eng. **139**, 282 (2001).

[40] A. N. Davletshin, E. V. Teplov, A. O. Tipunkov, S. V. Tikhonov, and V. A. Tolstikov (EXFOR 41183), Vop. At. Nauki i Tekhn., Ser. Yadernye Konstanty, Issue 1 (1993), p. 13.

[41] A. N. Davletshin, E. V. Teplov, A. O. Tipunkov, V. A. Tolstikov, I. A. Korzh, V. D. Ovdienko, N. M. Pravdivyy, N. T. Sklyar, and V. A. Mishchenko (EXFOR 41121), Vop. At. Nauki i Tekhn., Ser. Yadernye Konstanty, Issue 1 (1992), p. 41.

[42] R. P. Anand, H. M. Jain, S. Kailas, S. K. Gupta, and V. S. Ramamurthy (EXFOR 30781), Ann. Nucl. Energy **16**, 87 (1989).

[43] K. Kobayashi, Y. Fujita, and N. Yamamuro (EXFOR 21748), J. Nucl. Sci. Technol. **18**, 823 (1981).

[44] R. E. Chrien, H. I. Liou, M. J. Kenny, and M. L. Stelts (EXFOR 10793), Nucl. Sci. Eng. **72**, 202 (1979).

[45] W. P. Poenitz and A. B. Smith (EXFOR 10735), Technical report ANL-NDM-42, Argonne National Laboratory, 1978.

[46] R. L. Macklin and J. Halperin (EXFOR 10554), Nucl. Sci. Eng. **64**, 849 (1977).

[47] M. Lindner, R. J. Nagle, and J. H. Landrum (EXFOR 10221), Nucl. Sci. Eng. **59**, 381 (1976).

[48] M. Baba, H. Wakabayashi, N. Itoh, K. Maeda, and N. Hirakawa (EXFOR 22158), Technical report JAERI-M-89-143, p. 143, A.E.R.I, Japan, 1989.

[49] E. Sh. Soukhovitskiĭ, R. Capote, J. M. Quesada, and S. Chiba, Phys. Rev. C **72**, 024604 (2005).

[50] R. Capote, E. Sh. Soukhovitskiĭ, J. M. Quesada, and S. Chiba, Phys. Rev. C **72**, 064610 (2005).

[51] J. Raynal, Program ECIS03 (private communication, 2004).

[52] J. Raynal, in *Computing as a language of physics*, ICTP, International Seminar Course, Trieste, Italy, Aug. 2–10, 1971 (IAEA, Vienna, 1972), p. 281.

[53] W. Hauser and H. Feshbach, Phys. Rev. **87**, 366 (1952).

[54] H. M. Hoffmann, J. Richert, J. W. Tepel, and H. A. Weidenmuller, Ann. Phys. (NY) **90**, 403 (1975).

[55] O. A. Shcherbakov, A. Yu. Donets, A. V. Evdokimov, A. V. Fomichev, T. Fukahori, A. Hasegawa, A. B. Laptev, G. A. Petrov, Yu. V. Tuboltsev, and A. S. Vorobyev (EXFOR 41430), J. Nucl. Sci. Technol. Suppl. **2**, 230 (2002).

[56] B. I. Fursov, E. Yu. Baranov, M. P. Klemyshev, B. F. Samylin, G. N. Smirenkin, and Yu. M. Turchin (EXFOR 41111), At. Energ. (in Russian) **71**, 320 (1991).

[57] K. Kanda, H. Imaruoka, K. Yoshida, O. Sato, and N. Hirakawa (EXFOR 22014), Rad. Effects **93**, 233 (1986).

[58] J. W. Meadows (EXFOR 10843), Technical report ANL-NDM-83, Argonne National Laboratory, 1983.

[59] J. W. Behrens and J. C. Browne, Nucl. Sci. Eng. **77**, 444 (1981).

[60] J. Blons, C. Mazur, D. Paya, M. Ribrag, and H. Weigmann (EXFOR 21656), Phys. Rev. Lett. **41**, 1282 (1978).

[61] J. Blons, C. Mazur, and D. Paya (EXFOR 20796), Phys. Rev. Lett. **35**, 1749 (1975).

[62] M. Csatlós, A. Krasznahorkay, P. G. Thirolf, D. Habs, Y. Eisermann, T. Faestermann, G. Graw, J. Gulyás, M. N. Harakeh, R. Hertenberger, M. Hunyadi, H. J. Maier, Z. Máté, O. Schaile, and H.-F. Wirth, Phys. Lett. **B615**, 175 (2005).

[63] S. Ćwiok, W. Nazarewicz, J. X. Saladin, W. Plociennik, and A. Johnson, Phys. Lett. **B322**, 304 (1994).

[64] T. Belgya, O. Bersillon, R. Capote, T. Fukahori, G. Zhigang, S. Goriely, M. Herman, A. V. Ignatyuk, S. Kailas, A. Koning, P. Obložhinský, V. Plujko, and P. Young, IAEA-TECDOC-1506, Handbook for calculations of nuclear reaction data: Reference Input Parameter Library-2, available online at *http://www-nds.iaea.org/RIPL-2/* (IAEA, Vienna, Austria, 2006).

[65] S. Oberstedt, A. Oberstedt, F.-J. Hambsch, V. Fritsch, G. Lövestam, and N. Kornilov (EXFOR 22910), Ann. Nucl. Energy **32**, 1867 (2005).

[66] M. Petit, M. Aiche, G. Barreau, S. Boyer, N. Carjan, S. Czajkowski, D. Dassié, C. Grosjean, A. Guiral, B. Haas, D. Karamanis, S. Misicu, C. Rizea, F. Saintamon, S. Andriamonje, E. Bouchez, F. Gunsing, A. Hurstel, Y. Lecoz, R. Lucas, Ch. Theisen, A. Billebaud, L. Perrot, and E. Bauge, Nucl. Phys. **A735**, 345 (2004).

[67] B. I. Fursov, E. Yu. Baranov, M. P. Klemyshev, B. F. Samylin, G. N. Smirenkin, and Yu. M. Turchin (EXFOR 40837), At. Energ. (in Russian) **59**, 339 (1985).

[68] S. Plattard, G. Auchampaugh, N. Hill, G. De Saussure, J. Harvey, and R. Perez (EXFOR 10929), Phys. Rev. Lett. **46**, 633 (1981).

[69] D. W. Muir and L. R. Vesser (EXFOR 10223), Technical report LA-4648-MS, Los Alamos National Laboratory, 1971.

[70] S. M. Dubrovina and V. A. Shigin (EXFOR 40716), Dokl. Akad. Nauk **157**, 561 (1964).

[71] J. H. Williams (EXFOR 12300), Technical report LA-150, Los Alamos National Laboratory, 1944.

[72] K. Kobayashi, T. Kai, S. Yamamoto, H.-J. Cho, H. Yamana, Y. Fujita, T. Mitsugashira, I. Kimura, T. Yoshimoto, and Y. Ohkawachi (EXFOR 22647), Nucl. Sci. Eng. **139**, 273 (2001).

[73] K. Kobayashi, I. Kimura, H. Gotoh, and H. Yagi (EXFOR 20562), Technical report KURRI-TR-8, p. 10, Kyoto University Research Reactor Institute, Japan, 1975.

[74] F. Garcia, O. Rodriguez, J. Mesa, J. D. T. Arruda-Neto, V. P. Likhachev, E. Garrote, R. Capote, and F. Guzmán, Comp. Phys. Commun. **120**, 57 (1999).